From four- to six-coordinated silica: Transformation pathways from metadynamics

Roman Martoňák,[1,2,*] Davide Donadio,[2] Artem R. Oganov,[3,4] and Michele Parrinello[2]
[1]*Department of Experimental Physics, Faculty of Mathematics, Physics and Informatics, Comenius University, Mlynská dolina F2, 842 48 Bratislava, Slovakia*
[2]*Department of Chemistry and Applied Biosciences, Computational Science, ETH Zurich, USI Campus, Via Giuseppe Buffi 13, CH-6900 Lugano, Switzerland*
[3]*Laboratory of Crystallography, Department of Materials, ETH Zurich, Wolfgang-Pauli-Strasse 10, Zurich CH-8093, Switzerland*
[4]*Department of Geology, Moscow State University, 119992 Moscow, Russia*
(Received 10 January 2007; revised manuscript received 6 May 2007; published 27 July 2007)

We study transformation pathways leading from 4- to 6-coordinated silica using an improved version of the metadynamics method for the study of structural phase transitions in crystals [Martoňák, Laio, and Parrinello, Phys. Rev. Lett. **90**, 075503 (2003)]. The technique is able to simulate complex reconstructive structural transformations proceeding via number of intermediate states. In particular, we reproduce the experimentally observed crystal structures that are found upon pressurization of α-quartz. We also predict a low-energy transformation pathway from coesite to the metastable α-PbO_2 phase.

DOI: 10.1103/PhysRevB.76.014120 PACS number(s): 61.50.Ks, 64.70.Kb, 02.70.Ns, 07.05.Tp

I. INTRODUCTION

Silica (SiO_2) is an important system for geophysics and practical applications: it is the main component of the Earth's crust and is also of great relevance in materials science and technology. Its phase diagram is rather intricate and exhibits many different crystalline phases with different coordination of Si atoms. Silica is also known to exhibit a complex behavior under compression.[1–7] In particular, the outcome of the experiment was found to be strongly dependent both on the initial structure and on the details of the pressurization protocol. This indicates the presence of large kinetic barriers and metastability. Moreover, a propensity to amorphize upon compression has been reported.[8] At room temperature only the application of slow compression allowed phase transformations to crystalline phases to be experimentally observed. These transformations often proceed via metastable intermediates. For example, starting from α-quartz and using different experimental protocols, various phases have been found: transitions to poorly crystallized stishovite above 600 kbar,[2] to metastable quartz II at 220 kbar,[3] and more recently to a monoclinic $P2_1/c$ phase[5] at 450 kbar were reported. In all these cases the stable phase is tetragonal stishovite or its orthorhombically distorted variant, the $CaCl_2$-type phase. Upon application of pressure to coesite at room temperature only pressure-induced amorphization has been reported.[8] Similarly to experiment, theory is also faced with great difficulties, and our understanding of the complex transformation mechanisms is still incomplete despite a large number of simulations.[9–15] Polymorphism in silica was theoretically studied by total energy calculations[16–19] where the energetics of possible polymorphs are confronted or by molecular dynamics (MD) simulations using the Parrinello-Rahman method,[20] with empirical force fields[9–11,13,15] and with on-the-fly *ab initio* computed interactions.[12,14] However, static calculations have to rely on educated guesses on the possible structures, which may often be incorrect, and offer no clue as for the dynamics. Recently, thanks to the evolutionary algorithm USPEX,[21–23] it has become possible to find the stable crystal structure at given conditions without any empirical information or educated guesses. However, this algorithm cannot be used to find transition pathways. On the other hand, the strong metastability and the tendency of SiO_2 to amorphize present a problem in the dynamical studies. For example, in MD simulations starting from α-quartz the experimentally observed $P2_1/c$ phase and stishovite could not be observed. Therefore the gap between simulations and experiment is in this case quite large and points to the need for further development of simulation techniques.

In this paper we report the results of a study of pressure-induced transformations of silica using the improved version of the metadynamics-based approach.[24] Some preliminary results of this effort were already presented in Ref. 25. Here we provide a more detailed discussion of the method as well as more data from simulations. The paper is organized as follows. We first present in Sec. II an improved version of the metadynamics algorithm. In the following Section III we describe in detail the classical and *ab initio* simulations of pressure-induced transitions starting from α-quartz and coesite. Starting from α-quartz, we succeed in reproducing the whole experimentally observed sequence of pressure-induced phase transitions, including the final thermodynamically stable 6-coordinated stishovite. Starting from coesite we predict that it might transform into the metastable α-PbO_2 phase. We unveil the subtle and counterintuitive mechanisms of these transformations which often proceed via several intermediate states. Finally in Sec. IV we discuss some general aspects of this study and draw some conclusions.

II. METHODS

In Ref. 24 Martoňák, Laio, and Parrinello proposed a new scheme for simulation of structural phase transitions in crystals. Similarly to the Parrinello-Rahman (PR) method[20] it assumes periodic boundary conditions and uses the matrix **h**

formed by the simulation box edges $\mathbf{h}=(\vec{a},\vec{b},\vec{c})$ as collective coordinates that distinguish different crystal structures. In the PR method the matrix $\mathbf{h}$ is treated as a dynamical variable coupled to the microscopic degrees of freedom under the condition of constant pressure. At given pressure P and temperature T the system is always in a global or local minimum of the Gibbs free energy $\mathcal{G}(\mathbf{h})=\mathcal{F}(\mathbf{h})+PV$ ($V=\det\mathbf{h}$ is the volume of the supercell), which corresponds to a stable or metastable crystal structure, respectively. Due to the use of periodic boundary conditions and lack of heterogeneous nucleation centers, the barrier separating such minima is often much bigger than the thermal energy. This may result in artificial stability of the structures outside their thermodynamic stability range. In order to observe a structural transition within accessible simulation time, it is then necessary to set the pressure to values far beyond the thermodynamic transition pressure (over- or underpressurization). This may represent a substantial hysteresis which can prevent transitions to some phases and hide information about the kinetics of the phase transitions. Clearly, this has an adverse effect on the predictive value of the simulations. The metadynamics-based algorithm[24] cures this problem by introducing a mechanism enabling the system to cross the barriers. Following the general metadynamics method of Laio and Parrinello,[26] the technique[24] replaces constant-pressure simulation by systematic exploration of the Gibbs free energy surface constructed in such a way that it allows the system to find low-energy pathways from the initial to the final structure.

The original scheme[24] employs the matrix $\mathbf{h}$ directly as order parameter, requiring it to be in the upper triangular form in order to freeze unphysical box rotations.[27] It is convenient to define the six-dimensional order parameter as a vector $\tilde{\mathbf{h}}=(h_{11},h_{22},h_{33},h_{12},h_{13},h_{23})^T$. The metadynamics algorithm is then defined by the equations

$$\tilde{\mathbf{h}}^{t+1}=\tilde{\mathbf{h}}^{t}+\delta h\frac{\boldsymbol{\phi}^{t}}{|\boldsymbol{\phi}^{t}|}. \tag{1}$$

Here, the driving force $\boldsymbol{\phi}^t=-\partial G^t/\partial\tilde{\mathbf{h}}$ is derived from a modified Gibbs potential $\mathcal{G}^t$ which includes a history-dependent term,

$$\mathcal{G}^{t}(\tilde{\mathbf{h}})=\mathcal{G}(\tilde{\mathbf{h}})+\sum_{t'<t}We^{-|\tilde{\mathbf{h}}-\tilde{\mathbf{h}}^{t'}|^2/2\delta h^2}. \tag{2}$$

The history-dependent term[28] in $\mathcal{G}^t(\tilde{\mathbf{h}})$ pushes the system out of the local minimum. The first derivative of the Gibbs free energy with respect to the order parameter can be expressed as

$$-\frac{\partial\mathcal{G}}{\partial h_{ij}}=V[\mathbf{h}^{-1}(\mathbf{p}-P)]_{ji}, \tag{3}$$

and requires only an evaluation of the pressure tensor $\mathbf{p}$ by means of an ensemble average over a relatively short MD simulation.

The above version of the algorithm has been successfully applied to a number of systems.[29–33] In some cases, however, the use of the matrix $\mathbf{h}$ directly as the order parameter may not be convenient, since the shape of the free energy well in the $\mathbf{h}$ coordinates may be quite anisotropic. In addition to crystal anisotropy resulting in different stiffness with respect to the different components of $\mathbf{h}$, there is also a strong coupling among the components of $\mathbf{h}$. For example, the energy cost of a deformation where the system is compressed along all axes (volume compression) is typically much higher than the cost of a deformation where compression along one axis is compensated by expansion in the perpendicular directions (volume-conserving deformation). The basin of attraction of a crystal structure is therefore likely to be narrow in the direction of volume change and long in the perpendicular directions. Proper exploration of such valleys would require small Gaussians with respect to the narrow direction. Consequently, filling the well with such Gaussians would require a large number of metasteps, which is not practical. If the Gaussian size is not sufficiently small, the metadynamics algorithm does not guarantee that the system escapes from the basin of attraction of the initial crystal structure via the lowest-energy path. This is likely to be important in systems with complex free energy surfaces, where there are many competing pathways leading out of the initial free energy basin. Some of these pathways may lead to crystalline structures while others may result, e.g., in amorphization; there-

TABLE I. Eigenvalues (in units of kbar Å) and corresponding eigenvectors of the Hessian matrix (5) for a sample of α-quartz consisting of 324 atoms at temperature $T=300$ K and pressure $p=150$ kbar.

Eigenvalues					
2737.3	3318.8	8299.7	12102.3	18288.3	44790
Eigenvectors					
−0.0324	−0.3767	−0.0138	0.7446	−0.3698	−0.4070
0.0231	0.2932	0.0007	−0.4605	−0.6592	−0.5166
−0.0021	0.0075	0.0098	−0.0839	0.6522	−0.7533
−0.6852	0.0448	0.7269	0.0039	−0.0089	0.0036
−0.0500	−0.8764	0.0088	−0.4755	−0.0561	−0.0041
0.7255	−0.0442	0.6865	0.0185	−0.0059	−0.0007

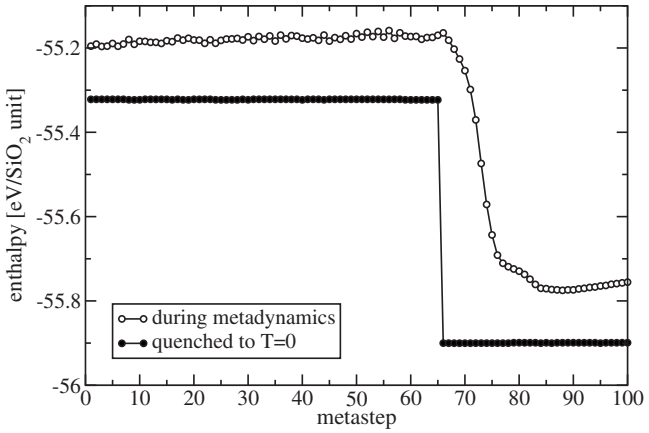

FIG. 1. Evolution of the enthalpy during metadynamics simulation of transition from α-quartz to quartz II at $p=150$ kbar. Enthalpy of configurations quenched to $T=0$ K at $p=150$ kbar is also shown.

fore it is important to perform the exploration of the free energy surface in a proper way so that the pathways crossing the lowest barriers are followed.

The shape of the bottom of the well is described by its curvature. Close to a given equilibrium crystal structure characterized by a matrix $\tilde{\mathbf{h}}^0$ the Gibbs free energy can be expanded to second order,

$$\mathcal{G}(\tilde{\mathbf{h}}) \approx \mathcal{G}(\tilde{\mathbf{h}}^0) + \frac{1}{2}(\tilde{\mathbf{h}} - \tilde{\mathbf{h}}^0)^T \mathbf{A}(\tilde{\mathbf{h}} - \tilde{\mathbf{h}}^0). \tag{4}$$

The Hessian matrix

$$A_{ij} = \partial^2 \mathcal{G}(\tilde{\mathbf{h}})/\partial \tilde{h}_i \partial \tilde{h}_j|_{\tilde{\mathbf{h}}_0} \tag{5}$$

can be calculated from the $\mathbf{h}$ matrix fluctuations in a constant-pressure simulation, or, alternatively, from the finite differences of the stress tensor at different values of $\mathbf{h}$, making use of Eq. (3). At equilibrium the $\mathbf{A}$ matrix has positive real eigenvalues $\{\lambda^i\}$ and can be diagonalized by an orthogonal matrix $\mathbf{O}$.

For illustration we show in Table I the eigenvalues and eigenvectors of the Hessian matrix (5) corresponding to a sample of α-quartz consisting of 324 atoms at temperature $T=300$ K and pressure $p=150$ kbar using the van Beest–Kramer–van Santen (BKS) force field[34] (see Sec. III A). We note the large spread of eigenvalues as well as the fact that the eigenvector corresponding to the largest eigenvalue points roughly along the direction (111000). Since for an upper triangular matrix the volume is simply expressed as $V=\det \mathbf{h}=\tilde{h}_1\tilde{h}_2\tilde{h}_3$, the direction of volume gradient in the $\tilde{\mathbf{h}}$ space is $\nabla V=(\tilde{h}_2\tilde{h}_3, \tilde{h}_1\tilde{h}_3, \tilde{h}_1\tilde{h}_2, 0, 0, 0)$ which is approximately parallel to the direction (111000) if the diagonal elements of $\mathbf{h}$ are not too different. In our experience this is typical, namely, the largest eigenvalue is associated with volume changes and is more than an order of magnitude larger than the smallest one.

In order to treat all degrees of freedom on equal footing it is convenient to diagonalize the quadratic form Eq. (4),

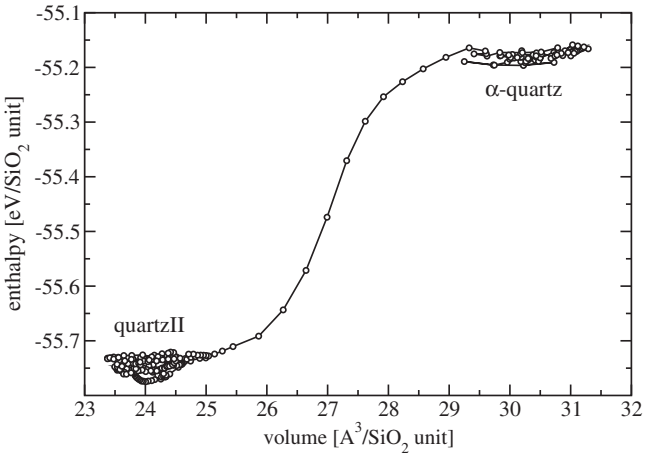

FIG. 2. Filling of the basins of attraction of two crystal structures during metadynamics. The horizontal axis corresponds to the volume, the vertical axis shows the enthalpy. Simulation started from α-quartz structure and was performed on a 324-atom sample at $T=300$ K and $p=150$ kbar.

which can be achieved by expressing the variables $\tilde{\mathbf{h}}$ in terms of new collective variables $\mathbf{s}$;

$$\tilde{h}_i - \tilde{h}_i^0 = \sum_j O_{ij} \frac{1}{\sqrt{\lambda^j}} s_j. \tag{6}$$

It is easily seen that in the new variables the well becomes spherical, $\mathcal{G}(\mathbf{s}) \approx \mathcal{G}(\tilde{\mathbf{h}}^0) + \frac{1}{2}\Sigma_i s_i^2$. The thermodynamic force $\partial \mathcal{G}/\partial s_i$ now reads

$$\frac{\partial \mathcal{G}}{\partial s_i} = \sum_j \frac{\partial \mathcal{G}}{\partial \tilde{h}_j} O_{ji} \frac{1}{\sqrt{\lambda^i}} \tag{7}$$

and can be easily calculated from the expression (3).

The metadynamics equations in the new variables read

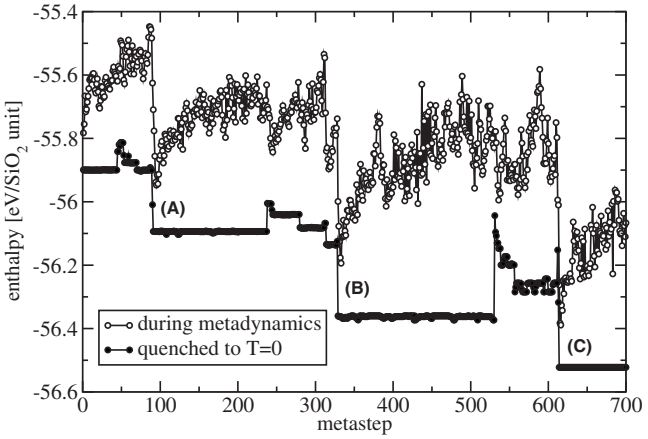

FIG. 3. Evolution of enthalpy during the metadynamics simulation started from the quartz II structure and performed on a 324-atom sample at $T=300$ K and $p=150$ kbar. Enthalpy of configurations quenched to $T=0$ K at $p=150$ kbar is also shown.

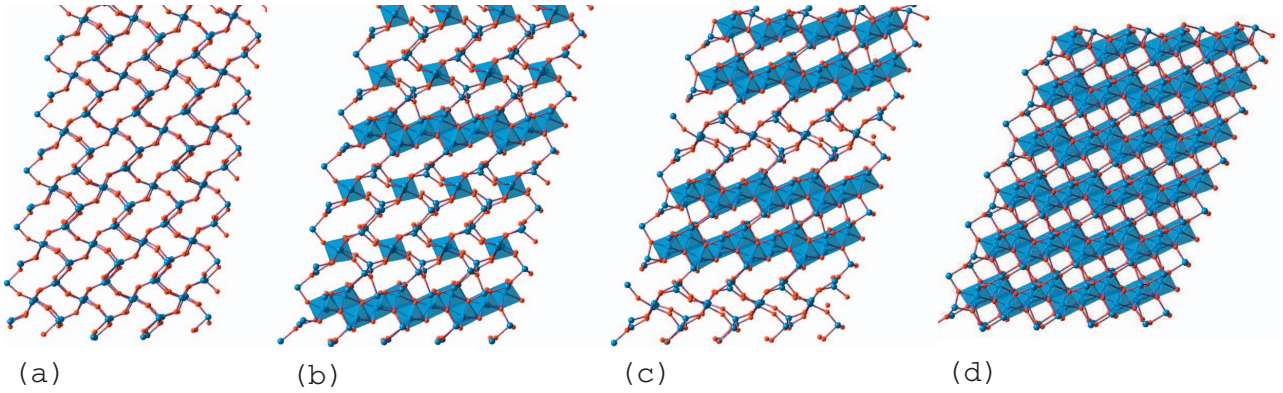

FIG. 4. (Color) Creation of the 3×2 kinked octahedral chains from quartz II at metasteps 85–92 (from left to right).

$$\mathbf{s}^{t+1} = \mathbf{s}^t + \delta s \frac{\boldsymbol{\phi}^t}{|\boldsymbol{\phi}^t|},$$

$$\mathcal{G}^t(\mathbf{s}) = \mathcal{G}(\mathbf{s}) + \sum_{t'<t} We^{-|\mathbf{s}-\mathbf{s}^{t'}|^2/2\delta s^2}, \tag{8}$$

where $\boldsymbol{\phi}^t = -\partial \mathcal{G}^t / \partial \mathbf{s}$. The width δs of the Gaussian is chosen such that its effect is substantially larger than the thermal fluctuation, i.e., $\delta s \gg \sqrt{k_B T}$. We shall use here the prescription of Ref. 24, which relates the Gaussian height W to the Gaussian width δs, in the form $W \sim \delta s^2$. A similar prescription was proposed in Ref. 35, in a different but related context.

Strictly speaking, it would be optimal to recalculate the Hessian matrix and redefine the coordinates every time the system undergoes a transition to a new structure. Since, however, the eigenvector corresponding to the largest eigenvalue is in most cases approximately parallel to the direction (111000), a set of coordinates calculated for the initial structure might still be usable for simulation of a series of transitions, since the separation between the direction of the volume gradient and the other degrees of freedom spanning the orthogonal subspace remains approximately preserved. When the bulk modulus of the system changes considerably, which is often the case when the system changes coordination, it is recommended to recalculate the Hessian matrix and continue metadynamics with new coordinates suitable for the new structure.

III. RESULTS AND DISCUSSION

In this section we present the results obtained by the application of the above technique to the study of the phase transitions at various pressures starting from α-quartz and coesite. These are two common four-coordinated phases of silica stable at room conditions and at elevated pressure, respectively. We choose to work at room temperature, where the free energy barriers for transitions are expected to be high. We analyze and describe in detail the transformation mechanism along the whole pathway from the initial to the final states which in some cases proceeds via a number of intermediate states.

Most of our extensive simulations were conducted using the BKS force field,[34] which has recently been shown to qualitatively reproduce the phase boundaries between quartz, coesite, and stishovite.[36] In our classical metadynamics simulations we employed the DLPOLY MD code.[37] We typically used for each metastep a 5–12 ps MD run, performing a constant volume and constant temperature simulation with the Berendsen thermostat,[38] equilibrating for 2.5 ps. In the *ab initio* calculations we adopted the Perdew-Burke-Ernzerhof generalized gradient approximation (GGA) functional developed by Perdew *et al.*[39] and norm-conserving pseudopotentials generated using the Troullier-Martins scheme.[40] In static calculations performed using the ABINIT package,[41] a plane wave basis set with a cutoff of 70 Ry was used. The total energy was integrated on Monkhorst-Pack[42] meshes of k points that guarantee a convergence within 10^{-5} hartree. The *ab initio* metadynamics was performed using the CPMD code,[43] the above-mentioned pseudopotentials, and a plane wave cutoff of 60 Ry. Each metastep consists of 5000 MD steps, which amounts to a simulated time of 0.75 ps. Different pseudopotentials have been used in the dynamical and the static calculations, and in both cases the convergence with respect to the plane wave basis set cutoff has been tested on the equilibrium structural and lattice parameters of α-quartz.

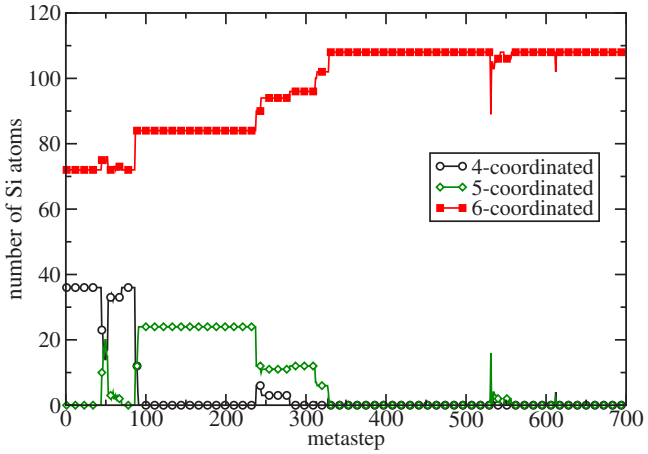

FIG. 5. (Color online) Evolution of the Si coordination number during metadynamics simulation starting from quartz II. Coordination number was calculated on configurations quenched to $T=0$ at $p=150$ kbar.

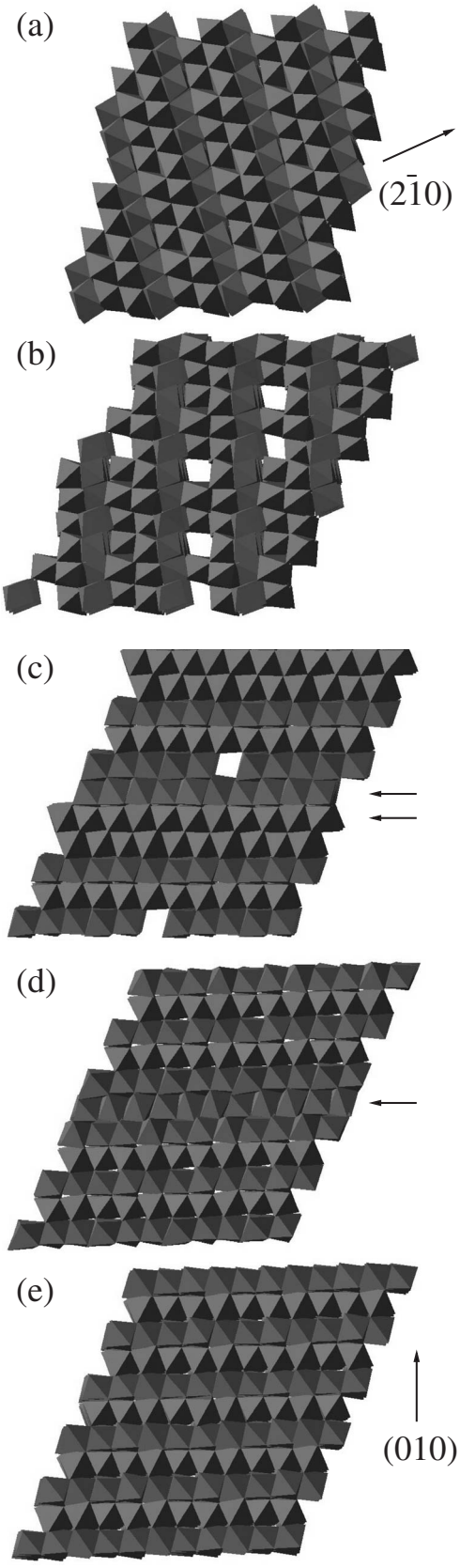

FIG. 6. Evolution of the stacking between metasteps 238 and 329. The arrows in (c) and (d) denote the planes that undergo rearrangement of stacking.

A. α-quartz under pressure

1. From α-quartz to quartz II

All simulations starting from α-quartz were performed with the BKS force field. We first applied metadynamics to a 324-atom supercell of α-quartz at $p=150$ kbar, where α-quartz is still mechanically stable, using $\delta s = 30$ (kbar Å^3)$^{1/2}$ and $W=900$ kbar Å^3. In order to get an idea of the free energy landscape visited during the metadynamics simulation, it would be useful to plot the time evolution of the Gibbs free energy. Since the latter is, however, difficult to calculate, in many cases it may be sufficient to neglect the entropic contribution and plot instead the enthalpy. For systems at temperature far below the melting temperature (such as silica at 300 K) enthalpy is likely to be a good approximation to the Gibbs free energy G. In Fig. 1 we show the time evolution of the enthalpy during the metadynamics run. The drop of the enthalpy occurring after 88 metasteps corresponds to the transformation of α-quartz to quartz II, which was also reported by other authors.[10,11,15,44] The transition is almost barrierless, and we verified that it is found even when metadynamics is performed at $T=0$. In order to identify the sequence of basins of attraction visited during the transition and reveal possible intermediate states, we quenched the final configuration of each metastep to $T=0$, keeping the external pressure at $p=150$ kbar. This procedure corresponds to local minimization of enthalpy in the spirit of the inherent structure analysis.[45] As can be seen in the figure the transition proceeds directly from the basin of attraction of α-quartz to that of quartz II and no intermediate states are present. In Fig. 2 we provide an alternative view, which shows the enthalpy as a function of volume in the course of metadynamics. This illustrates the process of filling of the initial basin of attraction and transition to a new one after crossing the barrier. In quartz II (space group $C2$) the Si atoms are arranged in alternating layers of tetrahedral and octahedral coordination and the transition is accompanied by a large volume drop (Fig. 2). The structural parameters of the $C2$ structure (as well as of the 3×2 and anatase structures discussed later in this section) optimized by *ab initio* calculations were presented as supplementary material in Ref. 25.

2. From quartz II to the 3×2 kinked structure

The partial change to octahedral coordination in quartz II is accompanied by a substantial increase of the stiffness of the crystal. We therefore decided to recalculate $\{\lambda_i\}$ and $\mathbf{O}$ and use in the continuation of the run collective coordinates appropriate for quartz II, with parameters $\delta s = 100$ (kbar Å^3)$^{1/2}$ and $W=2\times10^4$ kbar Å^3. In Fig. 3 the behavior of the enthalpy in the simulation starting from quartz II is shown. One can easily identify three different abrupt transitions which occur after rather high barriers are overcome. The quenched enthalpy also reveals the presence of a number of intermediate states visited by the system in the course of major transitions between large basins of attraction.

We start with the first major transition (A) taking place between metasteps 85 and 95. Quartz II is made of planes with ABC stacking in the (2$\bar{1}$0) direction with respect to the

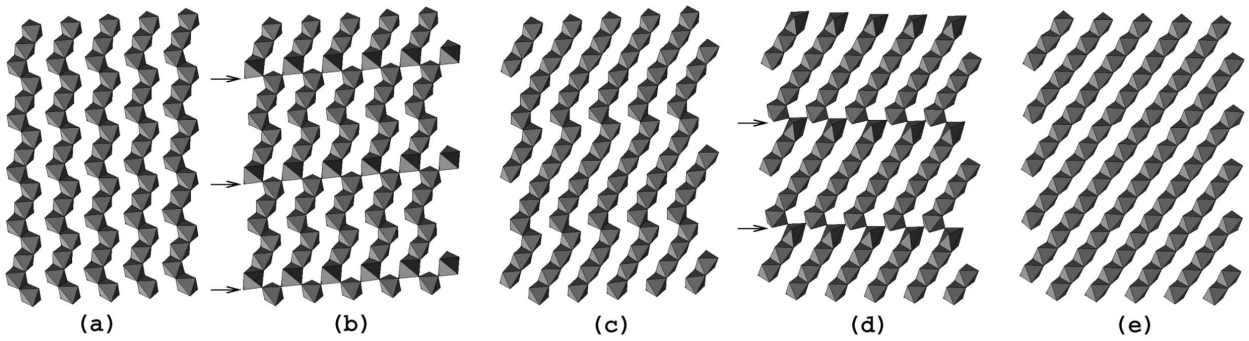

FIG. 7. Two steps of the transition from the 3×2 structure (a) to stishovite (e). Elimination of the kinking of octahedral chains proceeds via an intermediate 6×2 structure (c). The arrows denote the presence of corner-sharing octahedra in the transition states (b) and (d). After Ref. 25.

α-quartz reference supercell. The planes are made of octahedra and tetrahedra. In the course of the metadynamics run the three *ABC* planes transform into 3×2 planes, keeping the same stacking along the $(2\bar{1}0)$ direction. The octahedral dimers present in quartz II are split during this process as is shown in Fig. 4(a), which displays a pattern very similar to the one of α-quartz, with four- and sixfold channels. The 3×2 chains gradually appear [Figs. 4(b) and 4(c)] through the collapse of the fourfold channels into octahedral dimers. At the end of metastep 92 the structure is made of perfect 3×2 planes, but with an *ABC* stacking that does not allow full octahedral coordination, as is witnessed by the residual amount of fivefold coordinated silicon atoms (see Fig. 5). On the other hand there are no residual tetrahedrally coordinated silicon atoms. The five-coordinate state of silicon is potentially of great importance for transport and thermodynamic properties of high-pressure silicate melts; this exotic configuration can occur either dynamically (en route from fourfold to sixfold coordination), or in a metastable transition state (as we see here; see also Refs. 46 and 47).

The 3×2 pattern represents a particular case of a family of structures discussed in Ref. 17, where it was shown that low-enthalpy octahedral structures of silica at high pressure are characterized by chains of edge-sharing octahedra with various degrees of kinking and *ABAB* stacking of the octahedral planes. Therefore, after the transition A in Fig. 3, which leads to a structure with *ABC* stacking, another transition (B in Fig. 3) is needed to reach the lower-enthalpy structure with *ABAB* stacking. This occurs via a sequence of changes illustrated in Figs. 6(a)–6(e) and involves a change of the stacking direction from $(2\bar{1}0)$ [Fig. 6(a)] to (010). The rearrangement of the octahedral planes along the (010) direction occurs in the initial phase [Figs. 6(b) and 6(c)] and leads to a stacking that has the same periodicity as the simulation cell, which consists of six planes. We can assume that in larger systems this step leads to a random stacking, which is eventually reordered in the succeeding steps. When the new octahedral planes are created, the chains retain the 3×2 structure. The subsequent rearrangement of the stacking sequence in our simulation requires two steps [Figs. 6(c)–6(e)], in which the two planes indicated by the arrows in Figs. 6(c) and 6(d) are reoriented so that the correct *ABAB* stacking is finally obtained. At the same time this process removes the remaining coordination defects and the structure becomes fully octahedral (see Fig. 5).

By decompressing the structure from metastep 333 to $p=0$ and calculating its diffraction pattern, we found that it is identical to that corresponding to the $3\times2P2_1/c$ structure found experimentally in the recovered sample in Ref. 5, which belongs to the family of structures discussed in Ref. 17.

3. From 3×2 kinked structure to stishovite

During the filling of the basin of attraction of the structure B, the system creates some defects in one octahedral plane which appear as intermediate higher-enthalpy states on the quenched enthalpy curve between metasteps 531 and 612. Finally, the transition C starting at metastep 610 leads at metastep 616 to stishovite, which is the equilibrium structure at this pressure.[36] It is interesting to examine in detail how this transition takes place. In the $3\times2P2_1/c$ structure, the kink repeats itself every three octahedra [Fig. 7(a)] while stishovite is characterized by straight chains of octahedra [Fig. 7(e)]. The transition therefore requires elimination of the kinks. The path followed by the system is shown in Fig. 7, where two stages can be clearly identified. During metastep 612 [Figs. 7(a)–7(c)], the system eliminates half of the kinks and the structure of Fig. 7(c) corresponds to a 6×2 pattern. The transformation is based on a concerted bond-switch mechanism which occurs at the kinks and proceeds via a transition state [Fig. 7(b)], where the octahedra involved in the transition temporarily share their corners. This bond-switching process actually consists of two steps as illustrated in Fig. 8. The first bond switch causes the rotation of the octahedra at the kink of the chain, from the fully edge-sharing configuration within one chain to a corner-sharing configuration across two chains. The following step completes the rotation and makes the kink disappear. In the second part of the transition, which takes place at metastep 614 [Figs. 7(d) and 7(e)] the remaining kinks are eliminated and the chains become straight [Fig. 7(e)]. This transition also involves temporary formation of corner-sharing octahedra [Fig. 7(d)] via the bond-switching mechanism described above. The evolution of the supercell during the transitions at

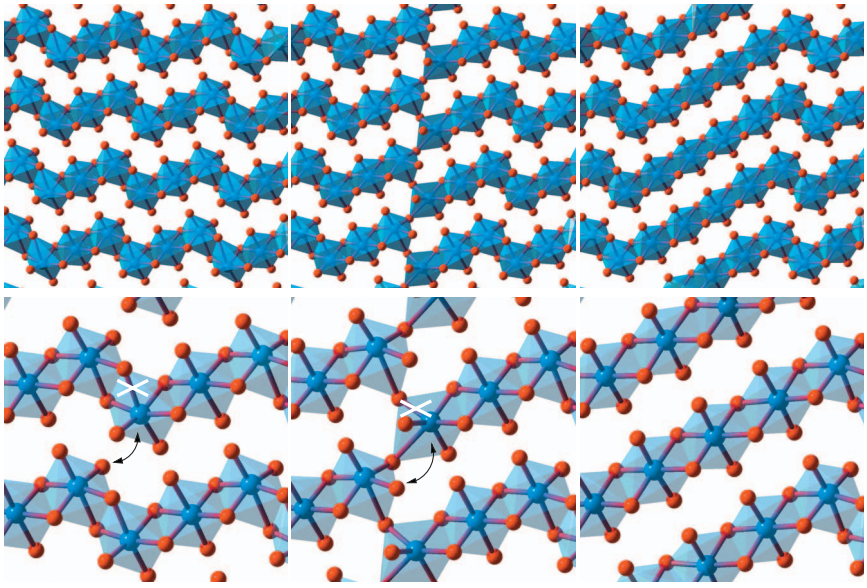

FIG. 8. (Color) Details of the bond switching mechanism at metastep 612 (from left to right).

metasteps 610–616 can also be viewed as a shearing mode in the (010) plane of stishovite, and only a tiny change of volume takes place. This agrees with Ref. 17, where it was stated that the kinked octahedral structures of silica have very similar volume; this conclusion naturally follows from the close-packing principle which describes these structures. An intuitive crystallographic pathway for such reconstructive transitions would involve an intermediate structure corresponding to a maximum common subgroup of the symmetry groups of the starting and final structures, usually involving small supercells.[48] For transitions between close-packed silica structures, such intuition would produce a mechanism based on nearly fixed oxygen atoms with the silicon atoms migrating into the empty octahedral voids. The transition mechanism we observe is very different: it occurs in two stages and involves crystallographic shear of large portions of the structure. We note that a similar mechanism was proposed for the postperovskite transition in $MgSiO_3$ (Ref. 31) from metadynamics simulations. The present work is the first case to our knowledge where MD simulations have been able to go beyond quartz II.

Finally, we illustrate the possibility of visualization of the metadynamics simulation in the order parameter space. While the visualization of the full six-dimensional free energy surface is not possible, in some cases it might be possible to identify a subset (one or two) of the six components of the vector **s** which undergo the most pronounced changes across the transition, while other components stay approximately constant. In this case one can plot, e.g., the Gibbs free energy or enthalpy vs two selected order parameter components as shown in Fig. 9. Here one can clearly see the basins of attraction of various structures, from initial quartz II to final stishovite, and follow their gradual filling during the simulation, as well as the respective transitions.

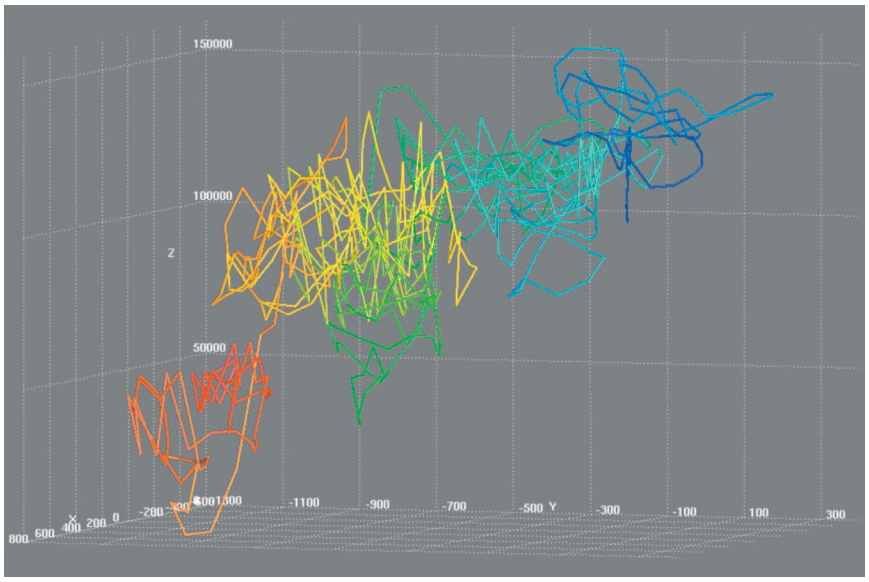

FIG. 9. (Color) Filling of the basins of attraction of several crystal structures during metadynamics. Horizontal axes correspond to components 3 and 5 of the order parameter **s**; the vertical axis shows the enthalpy. Units are arbitrary. Simulation started from the quartz II structure and was performed on a 324-atom sample at $T=300$ K and $p=150$ kbar. Color scale from deep blue to deep red corresponds to the metadynamics time.

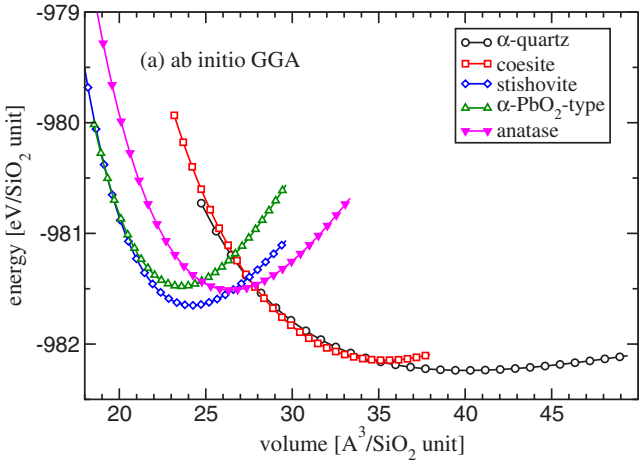

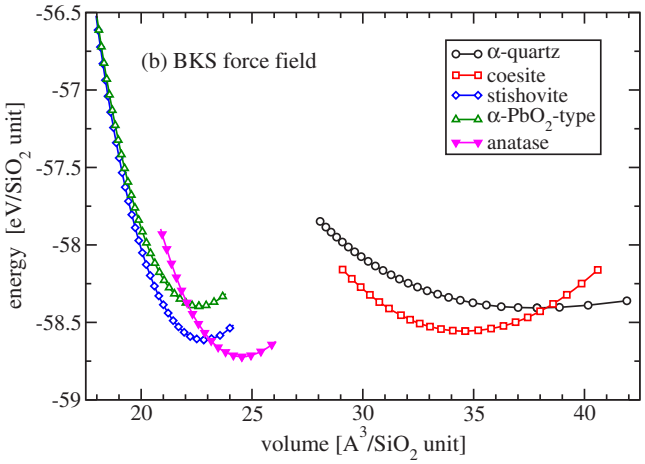

FIG. 10. (Color online) Equation of state of various silica phases from *ab initio* GGA (a) and BKS force field (b) calculations.

4. From α-quartz to anatase

We have repeated these calculations with a variety of cell sizes and slightly different pressures, also using different metadynamics parameters. As in real-life experiments the outcome is dependent on the protocol used. In some cases the simulation leads to an amorphous structure, in others to various defective phases with kinked chains or to a transition from α-quartz to quartz II followed by a direct transition to stishovite. The most surprising finding was a transition to an anatase structure ($I4_1/amd$), which so far has not been reported for silica. A static density functional theory calculation using a GGA exchange-correlation functional showed that the anatase structure, while having the lowest energy in a narrow range of volumes, is not the lowest-enthalpy phase at any pressure [see Fig. 10(a)]. However, since the energy of anatase is comparable to that of the other phases [Fig. 10(a)], it might perhaps be possible to prepare this phase experimentally as a metastable phase. In contrast, the same calculation performed with the BKS potential [see Fig. 10(b)] shows a phase boundary between coesite and anatase at −26 kbar and another one between anatase and stishovite at 102 kbar. The artificial stability of the anatase phase therefore represents a so far unknown artifact of the BKS potential. This finding demonstrates the excellent ability of our approach to find hitherto unexpected structures and suggests that this feature can be also used as a stringent test of model potentials.

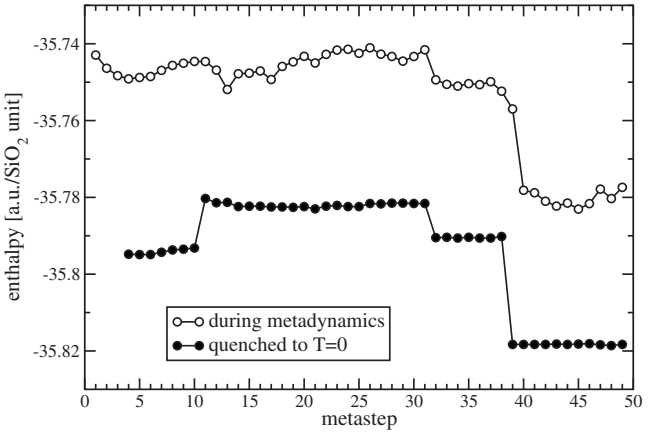

FIG. 11. Evolution of the enthalpy during the transition from coesite to the α-PbO_2 phase. *Ab initio* simulation was performed at $T=600$ K and $p=220$ kbar. Enthalpy of configurations quenched to $T=0$ K at $p=220$ kbar is also shown.

B. Coesite under pressure

Coesite is a complex tetrahedral structure with a conventional unit cell containing 48 atoms. We simulated a larger 192-atom cell with the BKS potential at 180 kbar, which is below the reported mechanical stability limit of 240 kbar for coesite within this model.[13] The simulation was repeated several times, and some of the runs resulted in transformation into the anatase phase but the dominant trend was toward amorphization. Given the fact that the BKS potential artificially favors the anatase phase we decided to repeat the simulation starting from coesite using metadynamics together with the *ab initio* Car-Parrinello scheme.[49] In this simulation performed at $T=600$ K and $p=220$ kbar we used the 48-atom unit cell and parameters $\delta s=40$ (kbar bohr^3)$^{1/2}$ and $W=1600$ kbar bohr^3. In 40 metasteps we found a transition from coesite to the metastable α-PbO_2 structure. The evolution of the enthalpy and structure is shown in Figs. 11 and 12. In Fig. 11 the enthalpy of the structures quenched to $T=0$ at $p=220$ kbar is also reported. The initial tetrahedral network topology of coesite [Fig. 12(a)] starts to change after the first ten metasteps. Threefold-coordinated oxygens are formed and the large rings from 9 to 12 members, that are characteristic for coesite, transform into smaller ones. As shown in Fig. 13, in this initial step all the fourfold-coordinated silicon atoms become five- and sixfold coordinated. Arrays of dimers of edge-sharing octahedra are formed and lie alternately in the (120) and ($1\bar{2}0$) planes, which are equivalent in the crystallographic structure of coesite [Fig. 12(b)]. This structure is obtained from a plastic deformation of coesite and is relatively stable at the present simulation conditions, as it corresponds to the local minimum at metastep 13 (see Fig. 11). It is, however, not stable upon decompression to $p=0$ and upon quenching the structure to $T=0$ at ambient pressure, coesite is recovered. In the

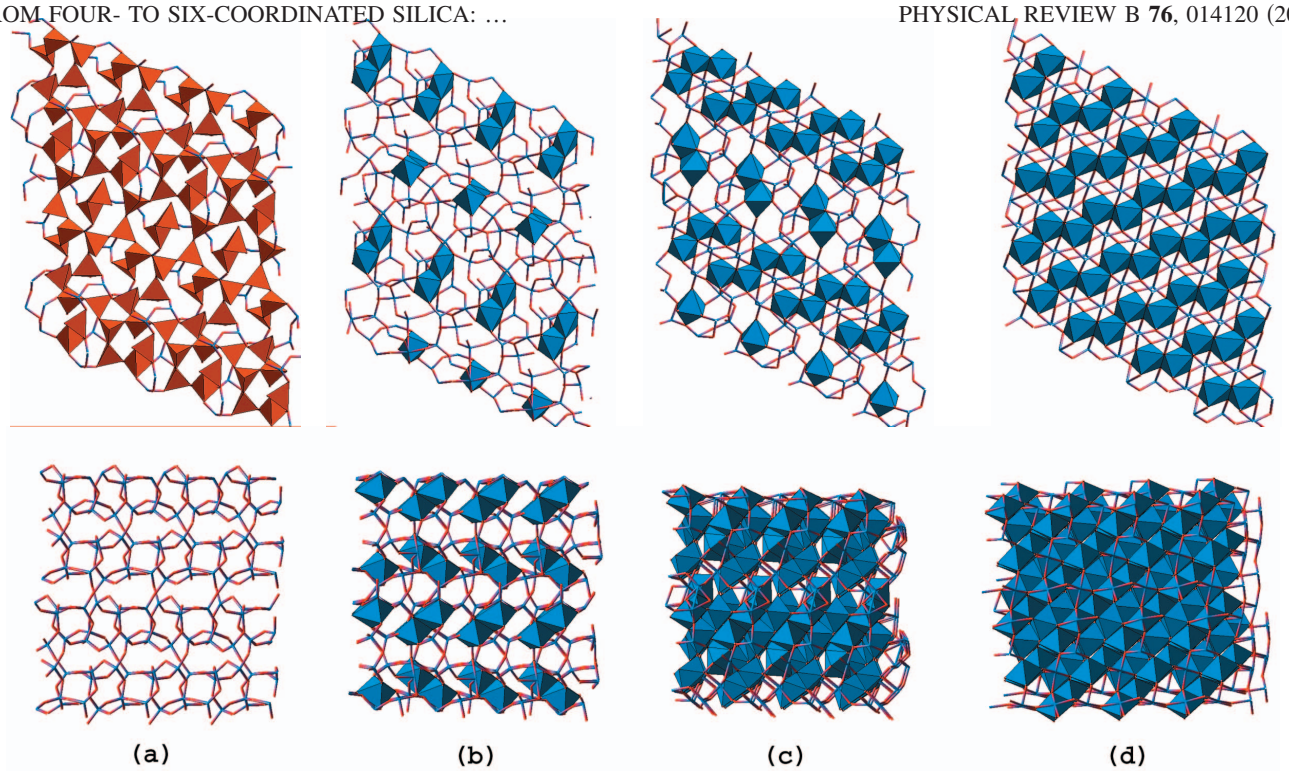

FIG. 12. (Color) Structural evolution during the transition from coesite (a) to the α-PbO_2 phase (d). Intermediate states (b) and (c) show the initial growth and competition of chains of octahedra in different planes. *Ab initio* simulation at $T=600$ K and $p=220$ kbar.

following metasteps more octahedra are formed and the planes grow until they interfere with one another. The arrangement of the octahedra at the transition state [Fig. 12(c)] already displays a preferred layering in the (120) plane, but several defects are present, as some chains of edge-sharing octahedra are still aligned in the competing symmetric $(1\bar{2}0)$ plane. The (120) planes display arrays of octahedra arranged in the 2×2 pattern characteristic of α-PbO_2, with remainders of misaligned octahedra. When the enthalpy barrier is overcome almost all the silicon atoms are sixfold coordinated and a slightly metastable intermediate is formed that survives for about six metasteps before the system turns into the α-PbO_2 structure. This intermediate has a defective α-PbO_2 structure with two undercoordinated silicon atoms in the 48-atom simulation cell. These defects do not recover upon decompression to ambient pressure. Finally, the enthalpy undergoes a large drop, the remaining coordination defects are eliminated, and a perfect α-PbO_2 structure is created. It consists of an *ABAB* stacking of (120) planes of edge-sharing octahedra arranged according to a 2×2 pattern[17] [Fig. 12(d)]. In another simulation at higher pressure (335 kbar) and room temperature, we observed that coesite is unstable, and rebinding already occurs during the structural optimization. Nevertheless, the same transition to the α-PbO_2 structure is found. Therefore we make the prediction that by appropriately modifying the experimental protocol a direct transition from coesite to the α-PbO_2 structure may be observed. We note that the transition from coesite to the α-PbO_2 structure is accompanied by a pronounced volume change of 24%, which is mainly achieved by a shrinking of the b axis ($\sim$15%). Therefore, in order to observe this phase transition experimentally, we suggest applying to coesite a uniaxial compression along the b axis.

IV. CONCLUSIONS

In this study we found several hitherto unknown transformation paths for structural transitions in silica polymorphs. Due to the efficiency of the improved metadynamics algorithm, it was possible to bring simulations much closer to thermodynamic conditions and also to much better agree-

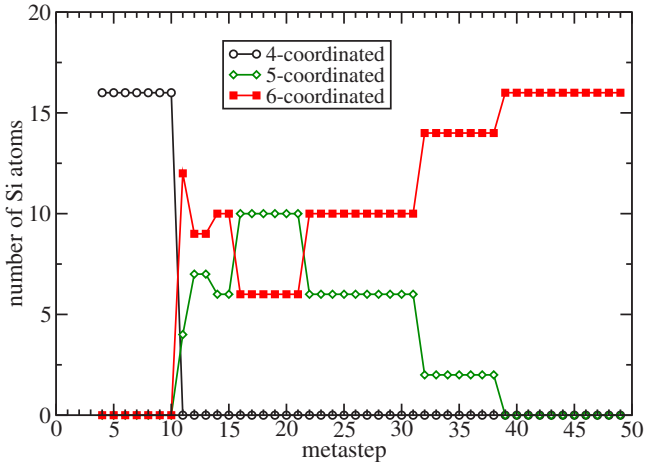

FIG. 13. (Color online) Evolution of the Si coordination number during the *ab initio* metadynamics simulation starting from coesite. Coordination number was calculated on configurations quenched to $T=0$ at $p=220$ kbar.

ment with experiment, and find an additional prediction.

Phase transition pathways, for which metadynamics gives useful predictions, are still very difficult to study experimentally. Yet it is the mechanism of the transition that determines its kinetic feasibility. Detailed understanding of these pathways and the associated kinetics is necessary for designing optimal routes for synthesis of metastable phases. For studies of structural transformations, the present method is far more efficient than previous ones, and finally brings the study of complex reconstructive structural phase transitions with many intermediate states within the reach of molecular dynamics simulations. This insight will help in designing new experimental protocols capable of steering the system toward the desired transition.

ACKNOWLEDGMENTS

We would like to acknowledge stimulating discussions with M. Bernasconi as well as help from P. Raiteri and M. Valle. R.M. was partially supported by Grant No. VEGA 1/2011/05 and Centre of Excellence of the Slovak Academy of Sciences (CENG).

*martonak@fmph.uniba.sk

[1] R. J. Hemley, C. T. Prewitt, and K. J. Kingma, in *Silica: Physical Behaviour, Geochemistry, and Materials Applications*, Reviews of Mineralogy Vol. 29 (Mineral Society of America, Washington D.C., 1994), p. 41.
[2] Y. Tsuchida and T. Yagi, Nature (London) **347**, 267 (1990).
[3] K. J. Kingma, R. J. Hemley, H. K. Mao, and D. R. Veblen, Phys. Rev. Lett. **70**, 3927 (1993).
[4] L. S. Dubrovinsky, S. K. Saxena, P. Lazor, R. Ahuja, O. Eriksson, J. M. Wills, and B. Johansson, Nature (London) **388**, 362 (1997).
[5] J. Haines, J. M. Léger, F. Gorelli, and M. Hanfland, Phys. Rev. Lett. **87**, 155503 (2001).
[6] L. S. Dubrovinsky, N. A. Dubrovinskaia, V. Prakapenka, F. Seifert, F. Langenhorst, V. Dmitriev, H.-P. Weber, and T. L. Bihan, Phys. Earth Planet. Inter. **143-144**, 231 (2004).
[7] Y. Kuwayama, K. Hirose, N. Sata, and Y. Ohishi, Science **309**, 923 (2005).
[8] R. J. Hemley, A. P. Jephcoat, H. K. Mao, L. C. Ming, and M. H. Manghnani, Nature (London) **334**, 52 (1988).
[9] S. Tsuneyuki, Y. Matsui, H. Aoki, and M. Tsukada, Nature (London) **339**, 209 (1989).
[10] N. Binggeli, J. R. Chelikowsky, and R. M. Wentzcovitch, Phys. Rev. B **49**, 9336 (1994).
[11] M. S. Somayazulu, S. M. Sharma, and S. K. Sikka, Phys. Rev. Lett. **73**, 98 (1994).
[12] R. M. Wentzcovitch, C. da Silva, J. R. Chelikowsky, and N. Binggeli, Phys. Rev. Lett. **80**, 2149 (1998).
[13] D. W. Dean, R. M. Wentzcovitch, N. Keskar, J. R. Chelikowsky, and N. Binggeli, Phys. Rev. B **61**, 3303 (2000).
[14] D. D. Klug, R. Rousseau, K. Uehara, M. Bernasconi, Y. Le Page, and J. S. Tse, Phys. Rev. B **63**, 104106 (2001).
[15] C. Campana, M. H. Müser, J. S. Tse, D. Herzbach, and P. Schöffel, Phys. Rev. B **70**, 224101 (2004).
[16] R. E. Cohen, in *Silica: Physical Behavior, Geochemistry and Materials Applications* (Ref. 1), p. 369.
[17] D. M. Teter, R. J. Hemley, G. Kresse, and J. Hafner, Phys. Rev. Lett. **80**, 2145 (1998).
[18] T. Demuth, Y. Jeanvoine, J. Hafner, and J. G. Ángyán, J. Phys.: Condens. Matter **11**, 3833 (1999).
[19] A. R. Oganov, M. J. Gillan, and G. D. Price, Phys. Rev. B **71**, 064104 (2005).
[20] M. Parrinello and A. Rahman, Phys. Rev. Lett. **45**, 1196 (1980).
[21] A. R. Oganov, C. W. Glass, and S. Ono, Earth Planet. Sci. Lett. **241**, 95 (2006).
[22] A. R. Oganov and C. W. Glass, J. Chem. Phys. **124**, 244704 (2006).
[23] C. W. Glass, A. R. Oganov, and N. Hansen, Comput. Phys. Commun. **175**, 713 (2006).
[24] R. Martoňák, A. Laio, and M. Parrinello, Phys. Rev. Lett. **90**, 075503 (2003).
[25] R. Martoňák, D. Donadio, A. R. Oganov, and M. Parrinello, Nat. Mater. **5**, 623 (2006).
[26] A. Laio and M. Parrinello, Proc. Natl. Acad. Sci. U.S.A. **99**, 12562 (2002).
[27] R. Martoňák, A. Laio, M. Bernasconi, C. Ceriani, P. Raiteri, F. Zipoli, and M. Parrinello, Z. Kristallogr. **220**, 489 (2005).
[28] T. Huber, A. E. Torda, and W. F. van Gunsteren, J. Comput.-Aided Mol. Des. **8**, 695 (1994).
[29] C. Ceriani, A. Laio, E. Fois, A. Gamba, R. Martoňák, and M. Parrinello, Phys. Rev. B **70**, 113403 (2004).
[30] P. Raiteri, R. Martoňák, and M. Parrinello, Angew. Chem., Int. Ed. **44**, 3769 (2005).
[31] A. R. Oganov, R. Martoňák, A. Laio, P. Raiteri, and M. Parrinello, Nature (London) **438**, 1142 (2005).
[32] T. Ishikawa, H. Nagara, K. Kusakabe, and N. Suzuki, Phys. Rev. Lett. **96**, 095502 (2006).
[33] D. Quigley and M. I. J. Probert, Phys. Rev. E **71**, 065701 (2005).
[34] B. W. H. van Beest, G. J. Kramer, and R. A. van Santen, Phys. Rev. Lett. **64**, 1955 (1990).
[35] H. Grubmüller, Phys. Rev. E **52**, 2893 (1995).
[36] I. Saika-Voivod, F. Sciortino, T. Grande, and P. H. Poole, Phys. Rev. E **70**, 061507 (2004).
[37] Computer code DL_POLY V2.14 (2003), W. Smith, M. Leslie and T. R. Forester, CCLRC (Daresbury Laboratory, Daresbury, Warrington WA4 4AD, England).
[38] H. J. C. Berendsen, J. P. M. Postma, W. F. van Gunsteren, A. DiNola, and J. R. Haak, J. Chem. Phys. **81**, 3684 (1984).
[39] J. P. Perdew, K. Burke, and M. Ernzerhof, Phys. Rev. Lett. **77**, 3865 (1996).
[40] N. Troullier and J. L. Martins, Phys. Rev. B **43**, 1993 (1991).
[41] X. Gonze *et al.*, Comput. Mater. Sci. **25**, 478 (2002).
[42] H. J. Monkhorst and J. D. Pack, Phys. Rev. B **13**, 5188 (1976).
[43] Computer code CPMD V3.9 Copyright IBM Corp. 1990–2004, Copyright MPI fuer Festkoerperforschung Stuttgart 1997–2001).
[44] N. Choudhury and S. L. Chaplot, Phys. Rev. B **73**, 094304 (2006).

[45] F. H. Stillinger and T. A. Weber, Science **225**, 983 (1984).
[46] R. J. Angel, N. L. Ross, F. Seifert, and T. F. Fliervoet, Nature (London) **384**, 441 (1996).
[47] A. R. Oganov, G. D. Price, and J. P. Brodholt, Acta Crystallogr., Sect. A: Found. Crystallogr. **A57**, 548 (2001).
[48] H. Sowa and E. Koch, Acta Crystallogr., Sect. A: Found. Crystallogr. **58**, 327 (2002).
[49] R. Car and M. Parrinello, Phys. Rev. Lett. **55**, 2471 (1985).